CHAPTER 1

Theory and Applications of NMR Spectroscopy in Biomolecular Structures and Dynamics of Proteins

KOUSIK CHANDRA,[a,†] ABDUL HAMID EMWAS,[b] SAMAH AL-HARTHI,[a] ZEYAD AL-TALLA,[c] DINA HAJJAR,[d] ARWA ABDULAZIZ MAKKI,[d] GHADA KHOUQEER[e] AND MARIUSZ JAREMKO*[a]

[a] King Abdullah University of Science and Technology (KAUST), Biological and Environmental Sciences & Engineering Division (BESE), Thuwal 23955-6900, Saudi Arabia; [b] King Abdullah University of Science and Technology. Core Labs, Thuwal 23955-6900, Kingdom of Saudi Arabia; [c] King Abdullah University of Science and Technology (KAUST), Ali I. Al-Naimi Petroleum Engineering Research Center (ANPERC), Thuwal 23955-6900, Saudi Arabia; [d] University of Jeddah, College of Science, Department of Biochemistry, Jeddah, Saudi Arabia; [e] Imam Mohammad Ibn Saud Islamic University (IMSIU), Riyadh, Kingdom of Saudi Arabia
*Email: Mariusz.jaremko@kaust.edu.sa

1.1 Introduction

Nuclear magnetic resonance (NMR) is a potent analytical technique with superior advantages, including its nondestructive nature, high reproducibility,

[†]These authors contributed equally.

New Developments in NMR No. 26
NMR Spectroscopy for Probing Functional Dynamics at Biological Interfaces
Edited by Anirban Bhunia, Hanudatta S. Atreya and Neeraj Sinha

Published by the Royal Society of Chemistry, www.rsc.org

and inherently quantitative methods.[1–3] The main strengths of NMR spectroscopy are that researchers can study a molecule at its atomic level, and several NMR measurements can be done on the same sample.[4–7] Thus, NMR can be used to identify and quantify different molecules within sample mixtures.[8–14] NMR can be utilized for molecular identification and elucidating different structures of the same molecule and hence is widely used in stereochemistry to identify different isomers of a molecule.[15–18] Moreover, coordination information on each atom and electron density and the memetic environments of neighbor's atoms can be extracted from the NMR spectrum.

The applications of NMR spectroscopy are no longer limited to the liquid state; it is now routinely used for solid states also.[19–25] Thus, NMR spectroscopy is broadly employed in a wide range of applications, including organic[26–32] and inorganic chemistry,[33–39] biology, physics,[40–46] and medical applications.[47–49] A simple one-dimensional (1D) proton NMR spectrum can be detected in a few minutes with minimal sample preparation, offering a high-throughput method appropriate for detecting the progress of organic reactions and for studies that include a large number of samples such as metabolomics and drug-discovery studies.[50]

One of the essential advantages of NMR spectroscopy is that samples can be detected under mild conditions without a vacuum or high temperatures. Researchers can measure NMR spectra separately by detecting selectively only one type of atom using 1D NMR experiments or the correlation between two types of atoms using 2D NMR experiments. Furthermore, the bond coordination of three or more different types of atoms can be detected using 3D and higher dimensional NMR methods.[51–53]

Indeed, one can carry out NMR measurements for biological molecules under physiological conditions such as body temperature, pH, and pressure. This was done first by Richard Ernst, who, based on an idea by Jeener, demonstrated two-dimensional (2D) NMR spectroscopy.[54,55] This opened up a new domain with many new experimental possibilities to obtain chemical shifts of coupled homonuclear and heteronuclear spins and the interactions between pairs of nuclear spins. This also forms the basis of the transfer of magnetization, which enables the basic building blocks for polarization transfer from one spin to another spin. The second breakthrough came from Anil Kumar, Ernst, and Wüthrich with the discovery of nuclear Overhauser effect experiments whereby spatial connections from adjacent spins to one spin are observed through the interplay of cross-relaxation and dipolar interactions between them.[56] This experiment and some other related 2D NMR experiments developed by the same group formed the basis for solving protein structures.

In 1985, the first protein structure of proteinase inhibitor IIA from seminal bull plasma was reported by the group of Wüthrich.[57] In the 1980s and 1990s, there was an explosive growth of high-resolution NMR in terms of developing new pulse sequences; instrument hardwire improvements in terms of higher magnetic fields, cryogenically cooled probes, *etc.*, and also better sample preparation, which involved the use of isotopically labeled proteins (^{1}H, ^{13}C, and ^{15}N). Slowly NMR became an increasingly powerful

technique for protein structure determination. Currently, about 10% of structures being deposited in the Protein Data Bank are solved using NMR. With an increase in dimensionality, measurement time increases rapidly, and there is constant effort to meet both the requirement of optimum sensitivity and desired resolution.

Over the past two decades, numerous advances have been made to achieve three- and four-dimensional (3D and 4D) spectroscopy in a reasonable amount of time.[58–61] There is an area of research for FAST NMR methodologies that have found profound application in the last two decades.[62,63] Perhaps the most exciting frontier is the application of NMR to investigate protein dynamics, especially for large molecular machines, which will undoubtedly lead to new fundamental insights in biology. NMR is the method of choice for dynamic molecular investigation; herein we focus on the theory and applications of different NMR approaches for biological molecules, focusing on protein dynamics. Since historical dynamics came first, we first discuss the basic theory and experimental details of protein dynamics. The details of structure elucidation follow this. Subsequently, we cover the recent development of the study of NMR dynamics, which includes structural information of sparsely populated states that are functionally most relevant.

1.2 Methodologies Involving Protein Structure Determination: A Comparative Study

As noted earlier, one of the most important advantages of NMR spectroscopy is the ability to elucidate the atomic-level structure of important biomolecules of interest, such as proteins.[64] Moreover, NMR is the only method that can be used for structural elucidation of biomolecules together with their complexes in solution under physiological conditions (with strictly defined temperature and pH, and ambient pressure). Thus, the determination of protein structure in its native environmental conditions is essential for a wide range of applications such as understanding protein functions, protein–protein and protein–drug interactions, and drug development. Initially, NMR experiments, such as 2D ^{1}H–^{1}H NOESY, were successfully applied to distinguish between the secondary structures of proteins.[65–68] Later, in 1982, the first-ever sequence-specific assignment for a small protein, basic pancreatic trypsin inhibitor, was published,[68] and this led to the determination of the first protein structure in solution in 1985.[57] Figure 1.1 shows how one can use NOESY data to distinguish an α-helix from other secondary structures.

The presence of secondary motifs within the protein structure is usually confirmed by the experimental data provided by NMR studies of peptides and proteins. The backbone vicinal coupling constants between amide protons NH and H^{α} protons [$^{3}J_{H_N H_\alpha}$] in the random coil are approximately equal to 7 Hz, which is close to the 8.5 Hz typical of β-sheets and far from the 4.2 Hz typical of an α-helix. In the case of the NOE (nuclear Overhauser effect), the random coil motifs exhibit strong sequential $H_\alpha(i)$ – $HN(i+1)$ effects typical of β-sheets, while $NH(i)$ – $NH(i+1)$ are fragile or not observed at all.[69–71]

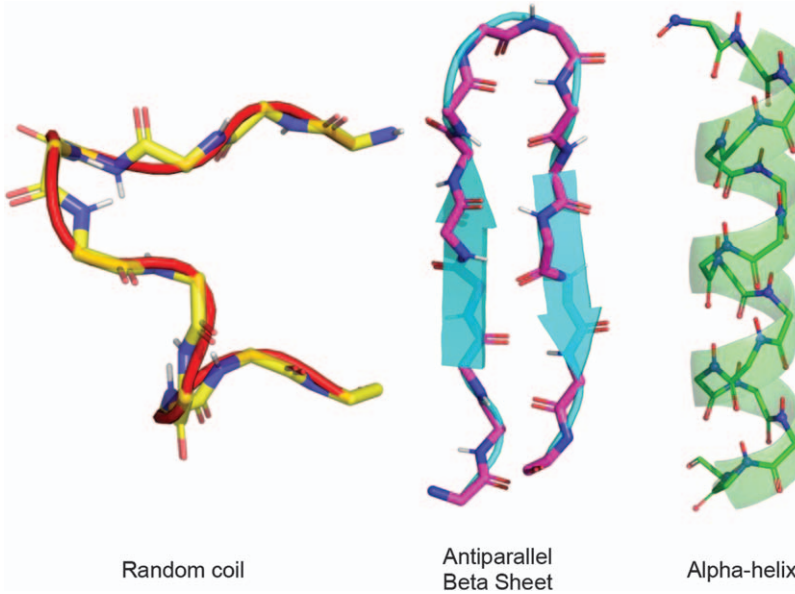

Figure 1.1 The secondary structures of protein highlighting the connectivity of interstrand NOEs.

Table 1.1 The distribution of protein and nucleic acid structures solved by currently available techniques. Data were taken from the Protein Data Bank (www.pdb.org), and the last update was May 17, 2021.

		Molecular type				
		Proteins (only)	Protein/NA	Nucleic acids (only)	Other	Total
Exp. method	X-Ray	138 515	7275	2172	149	156 318
	NMR	11 693	270	1358	31	13 389
	EM	5090	1738	58	3	7655
	Multiple methods	168	3	8	0	185
	Neutrons	69	0	2	0	71
	Other	32	0	1	0	37
	Total	155 567	9286	3599	183	177 655

Nowadays, the structures of different biomolecules solved by either NMR or other techniques are deposited in the Protein Data Bank (PDB) (website: www.pdb.org). There are over 300 000 structures of different biomolecules (of which 155 218 and 3594 are structures of proteins and nucleic acids, respectively) deposited in the PDB (April 29, 2021). Statistics of the PDB are presented in Table 1.1.

The relatively large disparity between the number of structures solved by NMR and X-ray techniques has several different causes, besides the fact that

NMR is a newer technique used in structural studies for important biomolecules. These causes include the following:

- The size limitation of objects suitable for NMR studies.[69] The average protein studied using NMR is *ca.* 100–150 amino acids long and requires double labeling. In proteins with over 180 residues, triple labeling with ^{2}H, ^{13}C, and ^{15}N isotopes is very often required. This is because the amount of information in spectra is too much and the relaxation behavior of larger systems that broaden the signal makes it difficult to detect and study.
- Relatively higher costs of protein production and measurements with the spectrometer.

The structure determination by NMR requires backbone and side-chain assignment as a prerequisite step. To achieve this, proteins need to be isotopically enriched. Isotope labeling requires cells expressing the protein in minimal media composed of ^{13}C-labeled glucose and ^{15}N-labeled ammonia salt. There can be an additional requirement of deuterium labeling for higher molecular size complexes or selective methyl labeling to resolve the highly overlapped methyl region. These requirements increase the sample production cost. Spectrometer hours are expensive because of relatively high cryo liquid consumption. The resonance assignment process typically involves recording multiple triple resonance experiments and other 2D and 3D experiments. The conventional method of recording experiments leads to higher time consumption. The analysis procedure is relatively tedious and time-consuming. The sample stability in solution is an issue as the sample should be stable for at least several weeks to complete the minimal set of multidimensional NMR experiments for assignment.

A tremendous amount of research has been carried out to overcome these difficulties, and these developments have led to different areas of research altogether. These developments are in different areas, such as ease of sample preparation, better labeling strategies, economically viable unlabeling strategies, improved hardwire settings, various fast NMR methodologies, *etc.* It is most common that researchers prefer to determine the high-resolution structure of their protein by X-ray, then assign only the protein backbone atoms with experiments based on NH detection, and study protein interactions and dynamics by solution-state NMR techniques.

In comparison to X-ray, NMR offers several possibilities that are not accessible to X-ray methodology. The most important advantages of NMR are:

- studying the protein structure in a native-like water environment;
- ability to test the impact of pH, temperature, ionic strength, and other factors on protein structure, stability, and interactions with ligands;
- studying protein dynamics in aqueous solutions (backbone by relaxation of ^{15}N atoms and side chains by ^{13}C-methyl relaxation);
- observation of chemical kinetics and estimation of thermodynamic parameters, binding constants, *etc*.;

- uncertainties of one type of experiment can often be resolved by different types of experiments done on the same sample, while in the case of X-ray, one crystal provides one consistent dataset that a different type of experiments cannot validate.

There are several routine steps in high-resolution protein structure elucidation based on multidimensional nuclear magnetic resonance techniques. First, when the target protein is known, and its molecular weight is under 20–25 kDa, and the expression protocol in *E. coli* is established, the following well-established scheme is usually applied:

1. Expression of the nonlabeled protein in *E. coli* in minimal M9 media (there are also other less common expression systems available, such as *Pichia pastoris* yeasts);
2. Defining the solution conditions, like buffer, pH, temperature, and salt concentration;
3. Expression of the double-labeled ^{15}N, ^{13}C protein in *E. coli* in minimal M9 media;
4. 3D experiments for backbone assignments and side-chain assignment;
5. Experiments delivering constraints for structure elucidation;
6. Determination of the structural constraints and structure calculation;
7. Structure validation and refinement.

The standard 3D experiments for double-labeled proteins for side chains and sequence-specific backbone assignments are based on HN-detected experiments. The protein solution usually contains 90%/10% H_2O/D_2O, which still allows for observation of the NH backbone and side-chain amides, locking the ^{2}H signal, but efficient suppression of the water peak at $\sim$4.7 ppm is required.[69] The experiments connecting the selected atoms of residues and between the residues are based on magnetization transfer on magnetically active nuclei.

For the sequence-specific backbone assignments, the simplest experiments used for double ^{15}N- and ^{13}C-labeled protein of MW under 20–25 kDa[69–72] are:

- 3D HNCA;
- 3D HN(CO)CA;
- 3D H(CA)NH;
- 3D HNCO;
- 3D HN(CA)CO;
- 3D CBCA(CO)NH;
- 3D CBCANH;
- 3D HNCACB.

The above-mentioned experiments are proton-detected ^{15}N-edited experiments where 2D [^{15}N, ^{1}H] HSQC serves as the fingerprint of the associated protein molecules. These experiments rely on one- and two-bond *J*

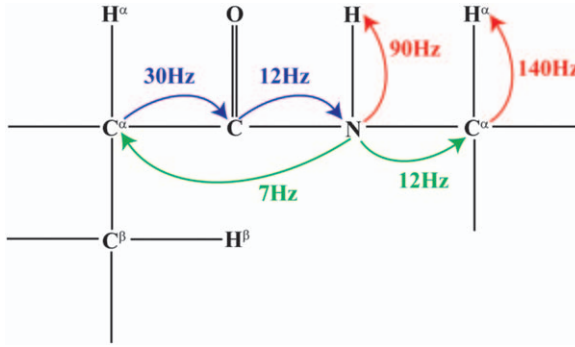

Figure 1.2 The approximate values of coupling constants between various backbone nuclei.

couplings, which are used to affect multiple magnetization transfer steps. The couplings are shown in Figure 1.2.

These couplings are largely independent of the backbone conformation of the proteins. However, there are changes in the values in the case of moving from proteins to nucleic acids. The nomenclature of the triple resonance experiments describes the associated magnetization transfer during the experiment, along with the frequency labeling. The nuclei, which are used only for transfer without frequency labeling, are kept in brackets. As an example, in the HNCO experiment, the magnetization starts from the $H^{N}_{(i)}$ proton and gets transferred through the directly attached $N_{(i)}$ atom to the $CO_{(i-1)}$ carbon atom and returns the same way to the $H^{N}_{(i)}$ nucleus. In HN(CA)CO, the magnetization passes through C^{α} atoms after nitrogen; however, the frequencies are not labeled. The detailed magnetization transfer pathways are presented in Scheme 1.1. All the experiments starting with HN are ''out and back'' experiments, while the last three experiments starting with $H^{\alpha/\beta}$ are ''out and stay'' experiments.

The magnetization transfer steps involve INEPT and will discuss the HSQC pulse sequence first in-depth, as it is the simplest of all, to understand INEPT and reverse-INEPT. Subsequently, we discuss in detail one triple resonance experiment.

The basic pulse sequence of HSQC is shown in Figure 1.3, which is composed of an INEPT sequence to transfer the magnetization from *I* to *S* spin. This is followed by the chemical shift evolution of *S* spin, during which I is decoupled by applying a 180° pulse in the middle. The last portion (c to d) represents the reverse INEPT block, which transfers the polarization back from *S* to *I*. Up to position a, *I* magnetization undergoes evolution under coupling, and an antiphase *I* magnetization (I_xS_Z) is generated. Simultaneous application of two 90° pulses makes it $I_zS_{x,}$ which is antiphase S magnetization. Thus, *I* magnetization is transferred to *S*. Subsequently, this antiphase term undergoes chemical shift evolution (Ω_S) for the t_1 period while the coupling is refocused by application of 180° *I* pulse at the midpoint of the evolution period t_1. Hence at position c, the coherence terms of

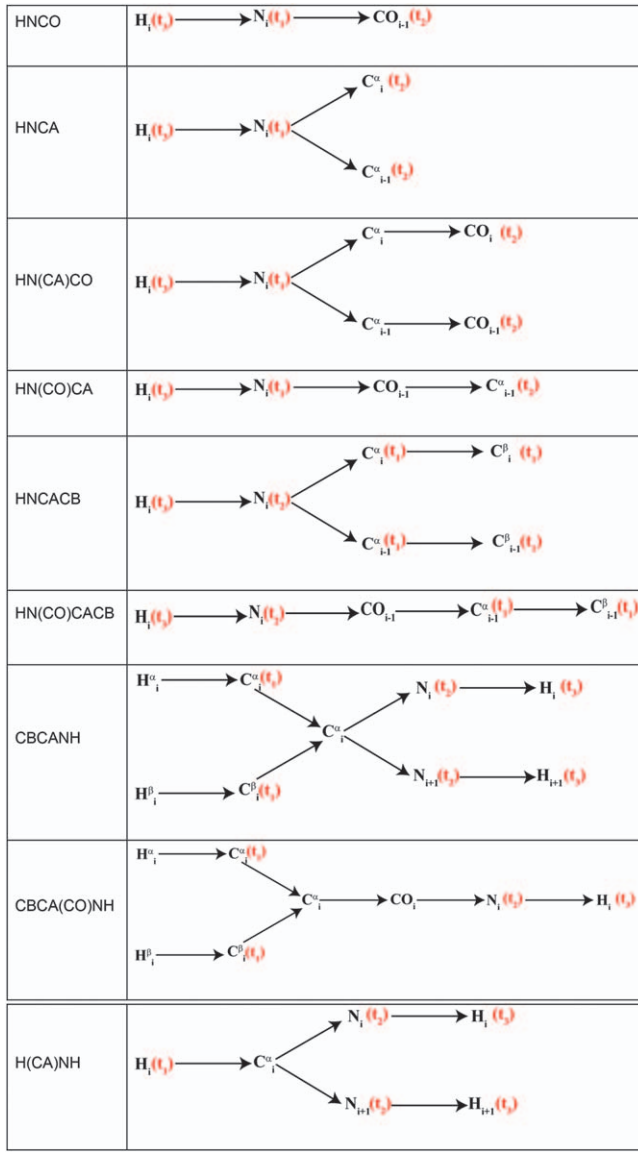

Scheme 1.1 The detailed magnetization transfer pathways for different experiments. (t_3) represents the detection dimension, while (t_1) and (t_2) represent the other two indirect dimensions in respective cases.

interest are $I_zS_x\cos\,\Omega_S t_1 + I_zS_y\,\sin\,\Omega_S t_1$. After this, the back INEPT starts, and two 90° pulses are applied. This results in the generation of $I_xS_x\,\cos\,\Omega St_1 + I_xS_z\,\sin\,\Omega St_1$. Among these two terms, the double quantum coherence (I_xS_x) is not observable. The second term encoded by antiphase I magnetization (I_xS_z) with sine modulation of S spin chemical shift becomes the

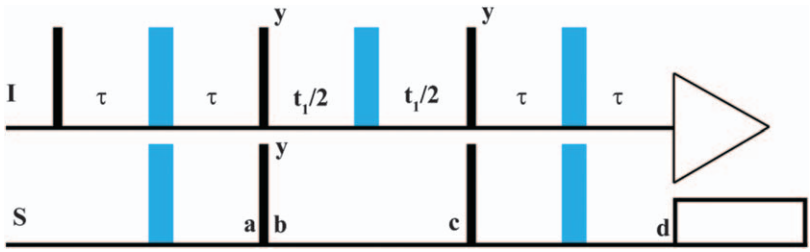

Figure 1.3 The pulse sequence of HSQC. *I* and *S* represent any two heteronuclear spins. The τ is $(1/4J)$, where J is the associated coupling constant. The thick blue and thin black bars represent the 180° and 90° pulses, respectively.

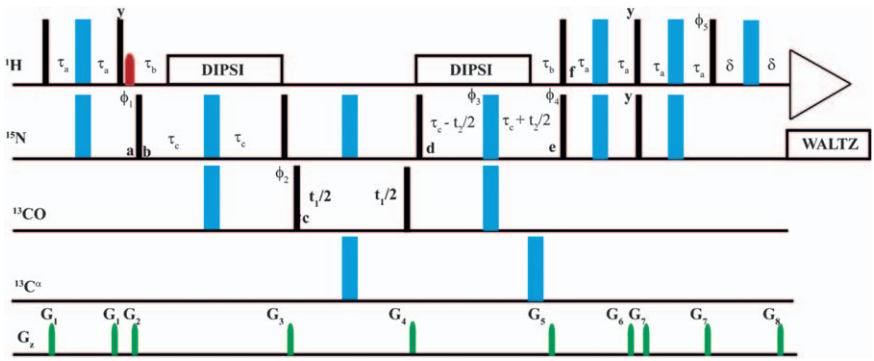

Figure 1.4 The pulse sequence of an HNCO experiment. Thin black bars and wide blue bars represent 90° and 180° pulses, respectively. The red-colored, shaped proton pulse is a water-selective 90° pulse. The DIPSI decoupling scheme is applied on the proton channel with lower power (5 kHz) compared to the hard pulse. The carbon pulses are applied as semiselective pulses. The transmitter offsets for the carbonyl and Cα carbon channels are set to 175 and 55 ppm, respectively. The coupling between the Cα and the nitrogen during chemical shift evolution of the nitrogen is removed by application of a single 180° pulse on Cα. The delays τ_a, τ_b, and τ_c are set to 2.3 ms $[1/(4J_{NH})]$, 5.5 ms $[1/(2J_{NH})]$, and 12.4 ms $[1/(4J_{NC})]$, respectively. The delay δ is required for the application and recovery of gradient G8 and is set to 0.5 ms. The phase cycle implemented is $\phi_1 = x, -x$; $\phi_2 = 4(x), 4(-x)$; $\phi_3 = 2(x), 2(-x)$; $\phi_4 = x$; $\phi_5 = x$, $\phi_{rec} = 2(x, -x), 2(-x, x)$. Gradients are usually sine-shaped with the following strengths and duration: G_1 (5 G cm^{-1}, 0.5 ms), G_2 (15 G cm^{-1}, 2 ms), G_3 (20 G cm^{-1}, 0.75 ms), G_4 (5 G cm^{-1}, 0.2 ms), G_5 (30 G cm^{-1}, 1.25 ms), G_6 (5 G cm^{-1}, 0.3 ms), G_7 (10 G cm^{-1}, 0.2 ms), G_8 (27.8 G cm^{-1}, 0.125 ms).

main interest. The antiphase term is evolved under J coupling for a period of $(1/2J)$ in order to generate in-phase I_y magnetization before detection at position d. During detection, the S spin is decoupled. Thus, in the ^{1}Hσ^{13}C/^{15}N HSQC experiments, the magnetization gets transferred from the more sensitive nucleus (I:^{1}H) to the less sensitive nucleus (S:^{13}C/^{15}N).

A detailed analysis using product operators is as follows (see Figure 1.4). Up to position b, ^{1}H magnetization goes through INEPT and gets transferred

to the nitrogen. Thus, the first pulse on the proton creates a transverse magnetization ($H_z \rightarrow -H_y$), which undergoes H–N coupling and generates antiphase magnetization ($2H_xN_z$). Subsequently, two 90° pulses on the proton and nitrogen channel generate the antiphase nitrogen magnetization ($2H_zN_y$).

In the next part of the sequence (from b to c), the magnetization evolves under different Hamiltonians containing evolution due to three different couplings: J_{HN}, J_{NC}, $J_{NC\alpha}$, and the nitrogen chemical shift. In this segment, only the J_{HN} and J_{NC} couplings evolve. Coupling evolution due to $J_{NC\alpha}$, and the nitrogen chemical shift evolution are refocused during this segment. The net result in this segment is that the antiphase proton-nitrogen magnetization is refocused to in-phase nitrogen magnetization ($2H_zN_y \rightarrow N_x$), and simultaneously, antiphase nitrogen-carbonyl carbon magnetization is generated ($N_x \rightarrow 2N_yC_z$). Since the Hamiltonians in NMR commute with each other, we can separately examine their effects, which is independent of how they are treated.

- Chemical Shift Evolution: The chemical shift evolution of the transverse nitrogen magnetization refocuses because the 180° nitrogen pulse is symmetrically placed during this time interval.
- Proton–Nitrogen Coupling: The coupling between the nitrogen and the amide proton is allowed to evolve for a period of τ_b. Subsequent application of the DIPSI decoupling prevents further evolution. Since τ_b is set to $1/(2J_{NH})$, the evolution due to this coupling ($2H_zN_y \rightarrow 2H_zN_y\cos(\pi J_{NH}\tau_b) - N_x\sin(\pi J_{NH}\tau_b)$) leads to pure in-phase nitrogen magnetization generation ($2H_zN_y \rightarrow N_x$).
- Nitrogen–Carbonyl Coupling: The coupling between the nitrogen and the carbonyl carbon occurs for the entire period as 180° pulses were applied to both spins. This leads to the generation of two terms from pure in-phase nitrogen magnetization;

$$N_x \rightarrow N_x\cos(\pi J_{NC}\ 2\tau_c) + 2N_yC_z\sin(\pi J_{NC}\ 2\tau_c).$$

Since $\tau_c = 1/(4J_{NC})$, only the antiphase term survives, which is $2N_yC_z$.

- Nitrogen–C^α Coupling: Since a 180° pulse is applied only to the nitrogen during this period, this coupling is refocused over the $2\tau_c$ period.

  In the following period (c to d), the first antiphase carbonyl magnetization is created by simultaneous application of a 90° pulse on the nitrogen and carbonyl channels ($2N_yC_z \rightarrow -2N_zC_y$). After this, the chemical shift for the carbonyl is recorded, and the following terms are generated.

$$-2N_zC_y \rightarrow -2N_zC_y\cos(\omega_C t_1) + 2N_zC_x\sin(\omega_C t_1)$$

  Out of these, only the cosine term is detectable. Thus, during the chemical shift evolution, the coupling with nitrogen and C^α is suppressed by applying the 180° pulses in the respective channel. Subsequently, the magnetization is transferred back to nitrogen by simultaneous application of 90° pulses at point d ($2N_zC_y\cos(\omega_C\ t_1) \rightarrow 2N_yC_z\cos(\omega_C\ t_1)$).

Subsequently, in the following period (d to e), antiphase nitrogen magnetization with respect to carbonyl is transferred to in-phase nitrogen magnetization with chemical shift labeling. Simultaneously, antiphase nitrogen magnetization is generated concerning the proton. The following terms are generated:

$$2N_yC_z \rightarrow -N_x \rightarrow -2N_yH_z$$

During this time, coupling with nitrogen and C^{α} is suppressed by applying the 180° pulse in the C^{α} channel. As a result, the effective coupling evolves for:

$$[t_C - t_2/2] - [\tau_C] + [t_2/2] = 0$$

From point e, back INEPT is initiated to the proton channel, which is brought in phase after sensitivity enhancement block and gets detected. This kind of analysis is possible for every triple resonance experiment.

Usually, the 3D ^{15}N NOESY-HSQC experiment is utilized, and the NH–NH connectivities, which are characteristic of α-helices, help validate the sequential assignments. For side-chain assignments, there are numerous different experiments, such as NH-detected:[70]

- 3D HBHA(CBCACO)NH;
- 3D (H)C(CO)NH;
- 3D H(CCO)NH;
- 3D 15N-edited TOCSY.

And CH-detected:[70]

- 3D (H)CCH TOCSY;
- 3D H(C)CH TOCSY.

These experiments utilize TOCSY transfer for complete side-chain assignment.

The 3D ^{15}N-edited NOESY experiment[73] and NH-NH connectivities characteristic of α-helices are successfully used for sequential residual assignment validation. Moreover, this experiment supplemented by 3D ^{13}C-edited NOESY can validate the side-chain assignments. It should be pointed out that ^{13}C-edited NOESY[74,75] is recorded separately for aliphatic and aromatic regions of the spectrum, with the $^1J_{CH}$ coupling constant and offset usually tuned to 140 Hz, 40 ppm and 160 Hz, 122 ppm for aliphatic and aromatic regions of the spectrum, respectively. Notably, the NOE contacts can also be successfully used for determining contacts between the residues placed in the interface of the relatively small oligomeric proteins. An example of such an application was demonstrated for a globular protein with a quaternary structure, the S100A1 protein, a dimeric protein consisting of two identical subunits forming a homodimer. As was shown by studies of a high-resolution NMR-based structure of human S100A1, and also bacterial CylR2 homodimeric proteins, the nature of the interactions within the interface of oligomeric proteins involves

mainly hydrophobic interactions between the methyl-containing side chains and several aromatic residues with weak C–H···π interactions.[76] An example of a weak intermolecular C–H···π interaction is between the aromatic moiety of Trp63 and the Hγ2/3 side-chain protons of Lys48, which is observed in the structure of the CylR2 dimeric protein.[77]

1.3 Through Space Correlation

The dipole–dipole interaction between two spins enables researchers to probe through space closed by atoms even though they are far apart in the primary sequence and usually from different spin systems (Figure 1.5). This phenomenon gives special significance for magnetic resonance spectroscopy in determining 3D structures of macromolecules such as proteins. There are different techniques to measure the distance between instigated spins, such as paramagnetic relaxation enhancement, **R**otational Frame **O**verhauser **E**ffect **S**pectroscop**Y** (**ROESY**), **N**uclear **O**verhauser **E**ffect **S**pectroscop**Y** (**NOESY**) and **H**eteronuclear **O**verhauser **E**ffect **S**pectroscop**Y** (**HOESY** or hetNOE). NOESY experiments are the most common approaches in biological structure analysis, mainly for protein structure elucidation. Hence, in this section, we present the theory and applications of different NOESY experiments. As most of the through-space correlations are based on the Nuclear Overhauser Effect (NOE) phenomenon, the basic concept of NOE will be presented first.

1.3.1 Nuclear Overhauser Effect

The Nuclear Overhauser Effect (NOE) phenomenon was discovered in 1953 by Albert Overhauser, who reported spin polarization enhancements by

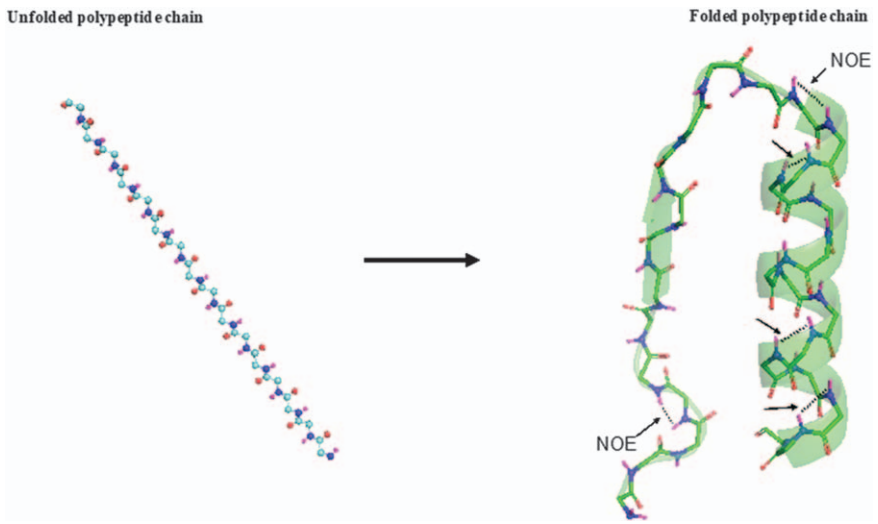

Figure 1.5 Folded and unfolded polypeptide chains highlighting the NOE effect.

microwave irradiation of conductive electrons in studied metals.[78] It can be defined as enhancing a spin's signal due to the transfer of magnetization from one nucleus to another through a cross-relaxation mechanism in a dipolar coupled system (through a space dipole–dipole relaxation effect).[79] As NOE occurs between different spins that are through-space coupled (dipole–dipole interactions), it provides important structural information.[80] Indeed, NOE has been used as a tool in NMR-based protein structural analysis for more than 20 years.[78,81] The NOE effect measures the distance between two nuclei within a short distance of less than 5 Å, therefore providing information on the identity of the atoms that are close together in space to help determine the intramolecular and intermolecular distances.[21] Such information can be obtained due to the folding of the protein (Figure 1.5), which detects the spins in proximity in space even though they are far apart in the primary sequence. As a result, the spins being irradiated will demonstrate the NOE effect independently from the direct connection of the spins by the chain of chemical bonds (scalarly or *J*-coupled). The NOE measurement is primarily used to provide information on the three-dimensional (3D) structure of biomolecules in solution by measuring the distances, and therefore calculating the global and local structures of the protein of interest. NOE has also been used to study macromolecular dynamics and is typically employed during the later stages of a structural investigation after the structure of the biomolecules has been fully defined by the use of different NMR experiments.

1.3.1.1 Basic Theory

The nuclei typically have two types of magnetic interactions: spin–spin interactions (scalar or *J*-couplings) and dipole–dipole interactions (dipolar couplings) and produce the NOE effect. The protein structure determination using NMR relies mainly on the NOE effect.[81–86] Theoretically, NOE is described as the change of signal intensity, either enhancement or decrease, of one spin when the transition of another is perturbed from its equilibrium population (Figure 1.6). This usually occurs by either inversion or saturation, eliminating a population difference between transitions that 2D-NOESY can visualize.

Dipolar relaxation is considered one of the most important sources of relaxation between the magnetic field of neighboring nuclei. For example, assume a system consisting of two spin-1/2 nuclei, *I* and *S* (*e.g.*, protons), where there is no scalar coupling (*J* for *I* and *S* is equal to zero), are spatially closed. This effect is described as cross-relaxation because spin *I* relaxes spin *S* and *vice versa*, resulting in alteration of the spin population. Therefore, this relaxation is distance-dependent, and the rate of relaxation that produces the NOE is inversely proportional to the sixth power of the distance between the interacting nuclei in space.[81]

$$I_{\mathrm{NOE}} \propto r^{-6}$$

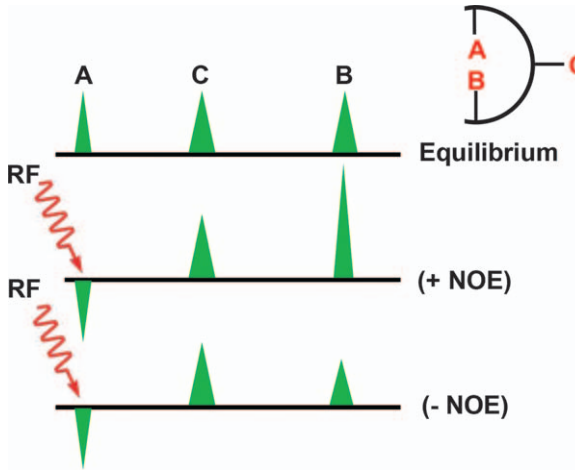

Figure 1.6 Nuclear Overhauser effect (NOE) for A and B, which are spatially close together, and A and C, which are far apart.

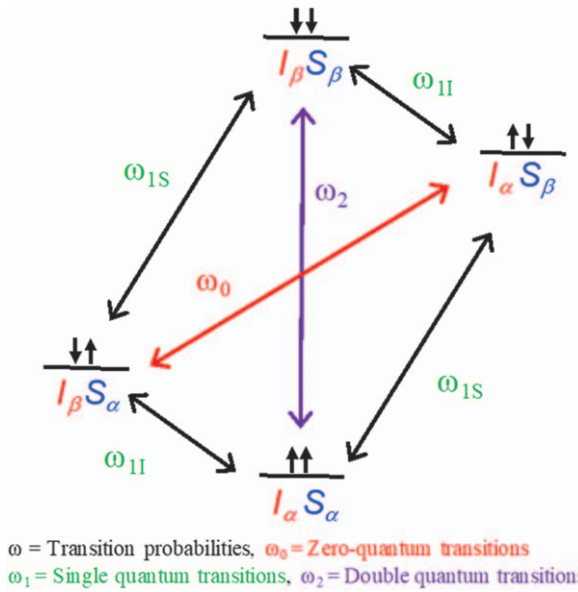

Figure 1.7 The four-spin energy level diagram and the six possible transitions of a two-spin system.

Figure 1.7 shows the energy level diagram and spin–flip transitions for the *IS* spin system, where the cross-relaxation that causes the NOE effect is represented. Such a system has four energy levels that depend on the spin-states of *I* and *S*, which correspond to αα, αβ, βα, and ββ, respectively. The dipolar interaction of the protons will cause T_1 relaxation between the spin states with the transition probabilities (ω). Notably, the ω's (ω_{1I}, ω_{1S}, ω_{0IS}, and ω_{2IS}) are

the probabilities per unit time of the nuclear spin-1/2 that a transition will occur between the spin energy states. In other words, the rates at which the corresponding spin flips occur. Thus, there are two single quantum transitions, ω_{1I}, corresponding to $\alpha\alpha \rightarrow \alpha\beta$ and $\beta\alpha \rightarrow \beta\beta$, and ω_{1S}, corresponding to $\alpha\alpha \rightarrow \beta\alpha$ and $\beta\alpha \rightarrow \beta\beta$, which is the normal transition probability that gives rise to a peak in the spectrum that requires frequencies or magnetic field fluctuations near the Larmor precession frequency. In addition, there is a zero-quantum transition, ω_{0IS}, corresponding to $\beta\alpha \rightarrow \alpha\beta$, and a double quantum transition, ω_{2IS}, corresponding to $\alpha\alpha \rightarrow \beta\beta$ that are collectively referred to as cross-relaxation pathways, which are responsible for the NOE effect.

When the spin is at equilibrium, this implies that the population of $\beta\beta$ is less than that of $\alpha\beta$, and the population of $\beta\alpha$ is less than that of $\alpha\alpha$ [Figure 1.8(A)].[87] When selective irradiation of the spin S is applied, it will cause the populations of the $\alpha\alpha$ and $\alpha\beta$, and also the $\beta\alpha$ and $\beta\beta$ states, to

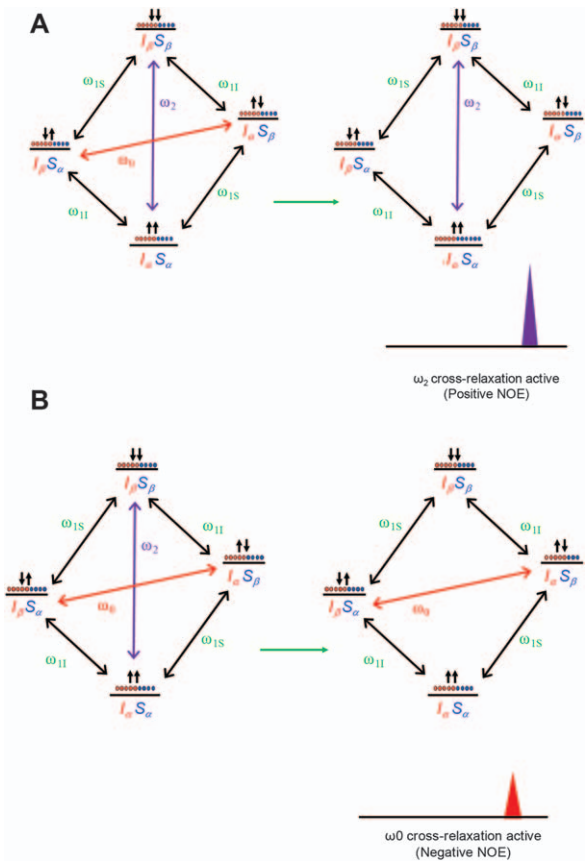

Figure 1.8 Schematic representation of population differences in energy levels of two spin system, S and I, that are dipolarly coupled. (A) after relaxation through the ω_2 process and (B) after relaxation through the ω_0 process.

become saturated (equalization of the α and β states of spin *S* through the single-quantum transition processes) [Figure 1.8(B)].[86] Then, as the relaxation takes place, the difference in these two populations depends on which possible relaxation processes dominates.[88]

First, domination by ω_1 (no NOE): upon *S* irradiation it will cause equalization of the populations of α- and β-spin states of *S*. Therefore, there will be no peak observed for *S* and because of the presence of only ω_1 relaxation ($\omega_2 = \omega_0$), spin *I* will be unaffected, which would lead to no NOE effect on *I* nuclei. Second, domination by ω_0 (negative NOE): now we consider the ω_0 process to be the only one that is operative. In the ω_0 process, when the *S* spin relaxes from the αβ to βα state, the *I* spin undergoes an $\alpha \rightarrow \beta$ transition. Thus, the population will flow from the αβ to the βα state. As *S* returns to its normal population difference, it will lower the population difference for *I*, resulting in a decrease in the *I* intensity as the *S* intensity decreases. If *S* is irradiated continuously, then the signal for *I* will vanish (−100% NOE). This is a negative NOE, which is more effective for slow tumbling rate molecules (large molecules). Third, domination by ω_2 (positive NOE): for the ω_2 process, when the *S* spin relaxes from the β to the α state, *I* spin transfers from ββ states to αα states, again in order to recover the population differences across the *S* transitions. This has the effect of increasing the population difference across the two *I* transitions, therefore increasing the intensity of the *I* spin in the spectrum. This is then a positive NOE, which is more effective for small molecules due to their faster tumbling rate in a solution.

The magnitude of this transition is expressed as a relative intensity change between the equilibrium intensity, according to the following equation:

$$N_1(S) = \frac{I - I_0}{I_0} \times 100(\%)$$

where $N_1(S)$ shows the NOE of spin *I* once it has been perturbed by spin *S*, *I* is the intensity in the presence of NOE, and I_0 is the equilibrium intensity.

1.3.1.1.1 Experimental Types. Based on the NOE method, many NMR techniques have been developed for protein structure determination including the widely used **NOESY**, **HOESY,** and hetNOE and **ROESY**.[89]

Nuclear **O**verhauser **E**ffect **S**pectroscop**Y (NOESY)**

The NOESY is the most common technique that is widely used in large molecules to determine the cross-correlation between similar nuclei (*e.g.*, ^{1}H–^{1}H) that are spatially close. The basic pulse sequence of 2D NOESY is presented in Figure 1.9 and follows similar principles to the homonuclear 2D experiments. After applying a 90° pulse, the transverse magnetization evolves during a free evolution t_1 period followed by a second 90° pulse that creates longitudinal magnetization.[79] The transfer of magnetization to other spins occurs during the mixing time (τ_m), through cross-relaxation, which eventually establishes the correlations. A final 90° pulse is then applied to create transverse magnetization, thus allowing the signal to be detected.

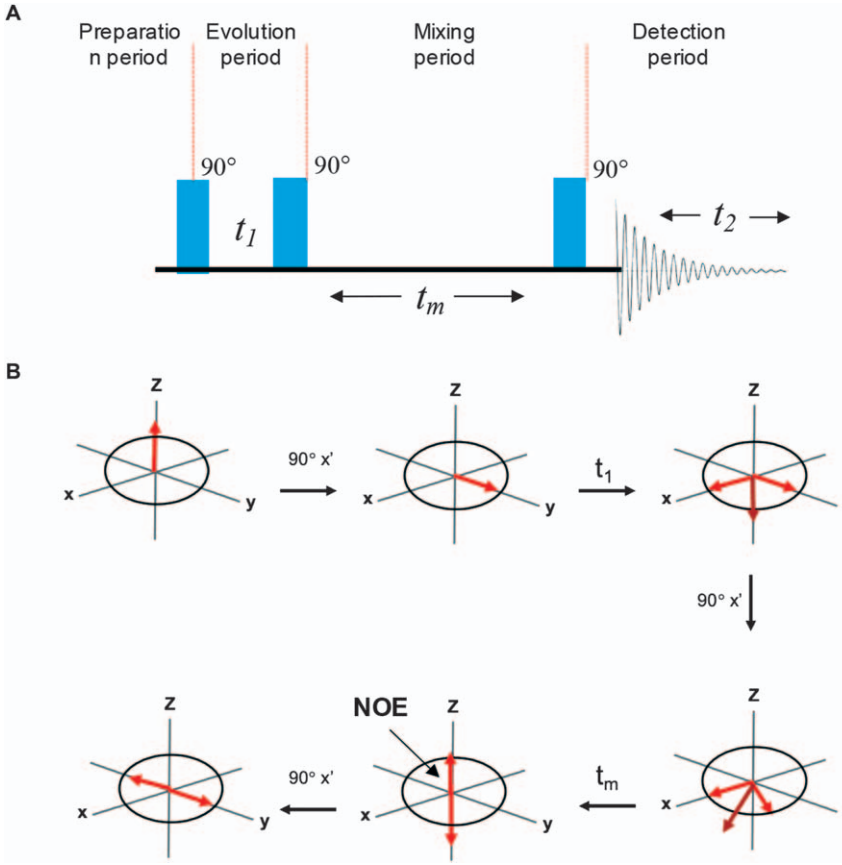

Figure 1.9 (A) The pulse sequences used to record classic 2D NOESY spectra. (B) A vector model describes ^{1}H spin magnetization.

In NOESY experiments, the cross-relaxation can be observed while magnetization is aligned along the *z*-axis.[74] The 2D NOESY spectrum typically shows diagonal and off-diagonal peaks (cross-peaks). The diagonal peaks usually indicate the proton peaks observed in the 1-D spectrum, whereas the cross-peaks represent the dipole–dipole interaction between nuclei that are close in space to one another showing NOE interactions between the correlated spins (<5 Å).[90] Both types of peaks can be either the same or opposite phases, depending on the magnitude of the rotational correlation time (τ_c) for the molecular size and, hence, the molecular weight.[90] The molecular correlation time (τ_c) is the average time needed for a molecule to rotate fully through an angle of 1 rad around any axis.[91] Thus, molecules with a faster tumbling rate will have a shorter correlation time, whereas slower tumbling molecules have a longer correlation time.[89] Between these extremes of molecular tumbling rates, the conventional NOE can become weak and even vanishingly small for the mid-sized molecules.[89] Therefore, the rotating-frame NOE

measurements play a vital role in such situations. The approximate relationship between the correlation time and molecular weight (MW, in Da) is as follows:

$$\tau_c \approx \mathrm{MW} \times 10^{-12}\ (\mathrm{S})$$

For instance, if the diagonal peaks are phased positively (and fully absorptive), the small-sized molecules that rapidly tumble have short correlation times and positive cross-relaxation rates, resulting in weakly negative 2D cross-peak intensities. In comparison, large molecules (*e.g.*, proteins) that exhibit slow tumbling have negative cross-relaxation rates, leading to intense positive cross-peaks in the 2D spectrum.[90]

Through qualitative assessment of distances, the relationship between the intensity of the cross-peaks and the internuclear distance has been categorized into three main groups based on NOE distance restraints.[92] The strong peaks correspond to the spins that are 1.8–2.7 Å apart, followed by the medium-intensity peaks, which reflect the spins that are 2.8–3.3 Å apart, and finally the weakest peaks for the spins that are 3.4–5.0 Å apart.[92] The NOESY experiment is a useful tool for identifying the stereochemistry of a molecule and the close-by residues that can be beneficial for sequence assignment in proteins.[88] NOESY can also be performed in a one-dimensional (1D) manner by the selection of individual resonances. However, the 2D NOESY experiment has a number of advantages compared to its counterpart 1D, including the simplicity for setting up, less time-consuming, and it can be used for both small and large molecules.

Additionally, such experiments are nonselective, NOE can be mapped in a single experiment, and essentially, the spectrum is easy to interpret in a qualitative manner.[90] These factors have made 2D-NOESY a favorite technique for structural chemists and biologists. However, protein structure determination by solution NMR depends on 3D NOESY spectra to provide interproton distance restraints, which are obtained from the intensity of cross-peak signals.[93] The 3D NOESY spectra provide better resolution, and therefore, it can be easier to assign and measure peak intensities (necessary for distance quantitation). The NOESY technique is applied to generate distance restraints in structure calculations, which consider the predominant source of macromolecular structural information in structural biology.

Heteronuclear **O**verhauser **E**ffect **S**pectroscop**Y** (**HOESY** or hetNOE)

The HOESY technique is the heteronuclear version of the NOESY and is used for cross-peaks between different nuclear species (*e.g.*, ^{1}H with ^{13}C) that allow the detection of heteronuclear through-space NOE connectives between nonbonded nuclei.[94] Figure 1.10(A) shows the general feature of pulse sequences used to record classic 2D HOESY, and Figure 1.10(B) shows the vector representation that describes the *I* spin magnetization. Let us consider a system consisting of two spins (*I* and *S*), where *I* represents ^{1}H and *S* represents ^{13}C, as an example. An initial 90° pulse on the *I* spin is applied to flip the *I* spins into the *x*–*y* plane where their components (α and β) precess during t_1. The spins precess according to the resonance frequencies of the chemically

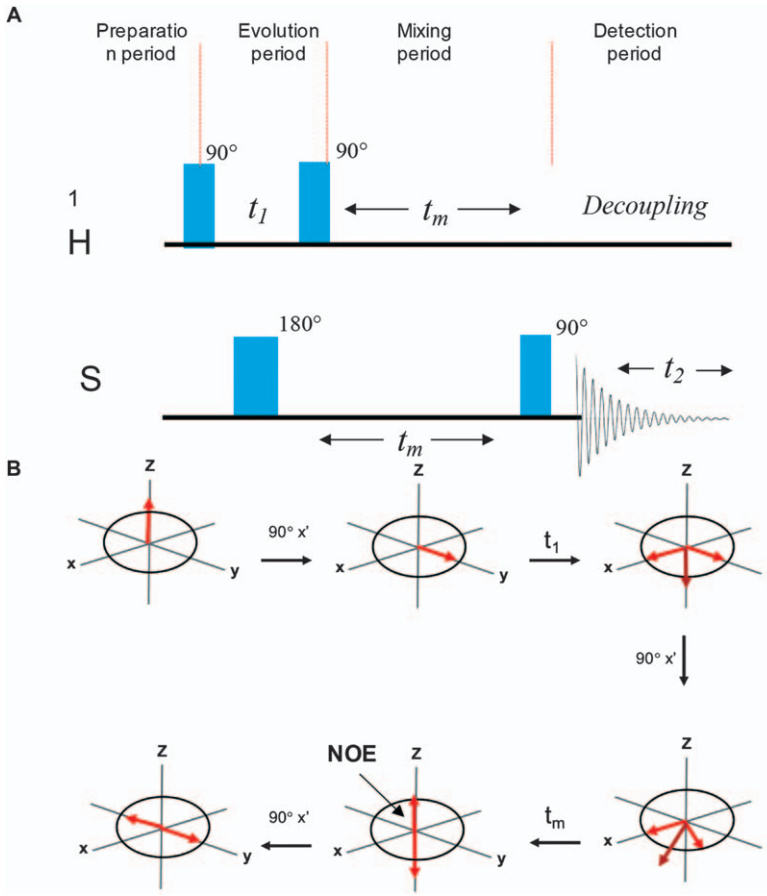

Figure 1.10 (A) The pulse sequences used to record classic 2D HOESY spectra. (B) A vector model describes *I* (^{1}H) spin magnetization.

distinct nuclei. Due to the coupling between the *I* and *S* spins, 180° pulse on the *S* spin at $t_1/2$ is applied to be removed. Then the spins precess for another $t_1/2$ period, resulting in refocusing of the two vectors. A second 90° pulse on the I spin creates longitudinal I spin magnetization followed by the mixing time (τ_m), where cross-relaxation leads to an exchange of magnetization between *I* and *S* spins through dipolar interactions. A final 90° pulse is then applied to create transverse magnetization for signal detection.

Rotational Frame **O**verhauser **E**ffect **S**pectroscop**Y** (**ROESY**)

ROESY, on the other hand, is typically used to obtain NOE information for mid-sized molecules that are approximately 1000–3000 Da in mass, such as peptides and small molecules, for which regular NOESY is not applicable. ROESY is especially suited for molecules with molecular correlation times (τ_c) such that $\omega_{\tau c} \sim 1$, where ω is the angular frequency $\omega = \gamma B$.[88] In such cases, the NOE for such molecules may be theoretically zero, so ROE (rotating frame

NOE) is often preferred since the ROE is always positive. In this technique, the homonuclear NOE effects are measured under spin-locked conditions, which involves using a spin lock to align the spins in the rotating frame where cross-relaxation occurs during the spinlock period (the mixing time, t_m).[90] For the 2D ROESY sequence, an initial 90° pulse is applied to put the net magnetization vectors (M) of the spins in the transverse (x–y) plane followed by a low-power RF spin-locking pulse for a time t_m during which magnetization transfer in the rotating frame occurs due to cross-relaxation (Figure 1.11).[95] The cross-peak generation occurs as the spins are held constant in the x–y plane and the magnetic field axis of the applied RF to prevent it from processing.[95] Under ROESY conditions, the mixing time (t_m) is typically 200–500 milliseconds depending on the T_2 of the sample, which is sufficiently long in the case of small molecules. As the ROESY pulse sequence is similar to TOCSY (Figure 1.11), it is essential to run ROESY with different mixing times. In general, the mixing time for TOCSY correlation is around 100 ms, while the ROESY ones are within 300–500 ms. Thus, running ROESY at different mixing times enables researchers to separate ROESY cross peaks from TOCSY ones. In the ROESY

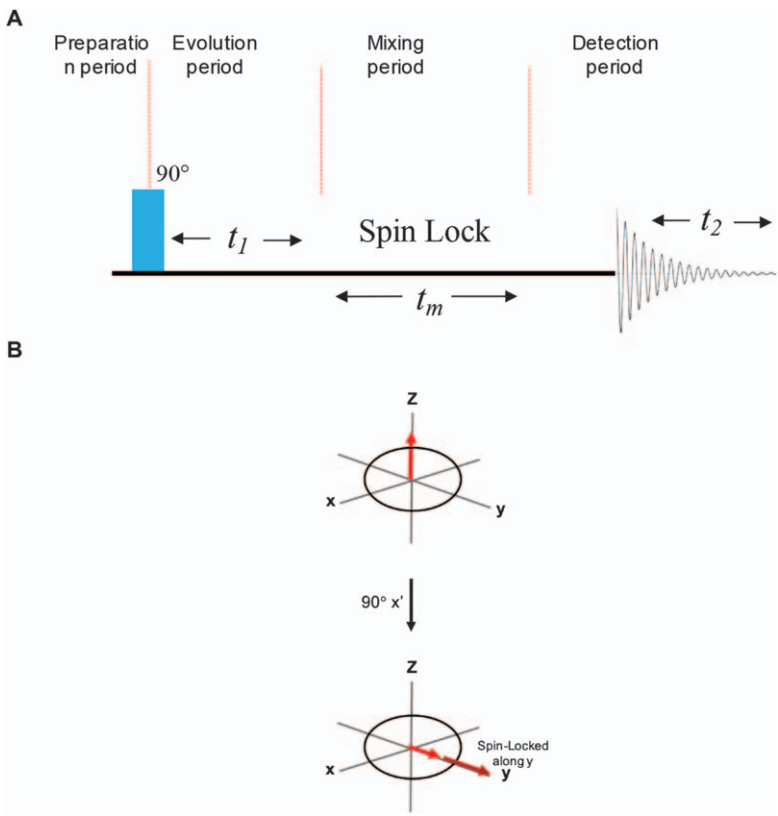

Figure 1.11 (A) The pulse sequences used to record classic 2D ROESY spectra. (B) A vector model describes ^{1}H spin magnetization.

spectrum, cross-peaks always have a sign opposite to the diagonal peaks, irrespective of the molecular weight. Such a technique is extensively used for small molecules such as saccharides, but is rarely used for proteins.

In comparison to NOESY, the main disadvantages that are associated with ROESY experiments are the lower sensitivity. Moreover, sample heating (specifically the ones in salty solutions) due to the requirement of spinlock during the mixing time can affect the molecular dynamics.[95] However, with small molecules, the trade between the negative and positive NOE effects can be comparable, leading to canceling of the NOE effects and cross-peaks of coupled spins will be undetectable, while the effect is always positive in ROESY experiments where all the cross-peaks would be detected.

1.3.1.1.2 3D NOESY Experiments. The use of solution NMR for the determination of protein structure has become a well-established technique. However, an increasing number of challenges may be encountered due to the size of the protein. Regularly, proteins with masses greater than 10–12 kDa with slower tumbling rates will display line broadening, causing a spectral congestion, which is an overcrowded rich peaks spectrum.[96] As a result, a signal overlap occurs even with the increase of the two-dimensional spectra resolution. For such proteins, both spectral crowding and rapid transverse relaxation can impair the analysis of cross-peaks in NOESY spectra that provide interproton distance restraints for structural models, therefore they can produce a spectrum that is impossible to assign.

To improve the resolution and overcome signals overlap, since it can be a major obstacle in the analysis of NMR spectra, three- and four-dimensional techniques have been developed to allow the possibility to study macromolecules up to 30 kDa in size.[97] The pulse sequence of a 3D experiment is changed to add a vertical domain, thus the information is spread into a third dimension resulting in a spectrum that can be visualized as a cube instead of a plane (usually ^{15}N or ^{13}C).[98] The 3D techniques are a natural progression of the 2D experiments so they are constructed from two 2D experiments combined, resulting in a spectrum that contains two evolution and two mixing periods that are inserted between the first mixing period and the direct data acquisition.[88,98] Each of the different indirect periods (t_1, t_2) is incremented separately.[88] Such a technique can aid in resolving the overlapped cross-peaks that show in a 2D spectrum. 3D NOESY NMR experiments can be categorized into two categories. The first is homonuclear NMR experiments where all three axes exhibit the same chemical shift of the same nucleus. They are rarely recorded due to the two transfer steps that would increase the number of possible correlations in the three-dimensional space.[98] The second is heteronuclear NMR experiments, which exhibit two or three different nuclei on the three axes and exhibit an increase in resolution due to the third dimension that is not compromised by an increased number of correlations.[98] The most widely used for structure determinations by solution NMR is heteronuclear-edited NMR experiments, such as 3D NOESY-HSQC (or HMQC), which can assist in spreading out of the signals by

combining HSQC and NOESY in a single 3D experiment by addition of the HSQC step into the NOESY pulse sequence.[69] Alternatively, acquisition starts after the HSQC step rather than at the end of the NOESY mixing time. $^{1}H–^{1}H$ NOESY spectra are edited by ^{15}N or ^{13}C chemical shifts. ^{15}N-edited 3D NOESY can exhibit peak overlap and symmetry problems, thus uncertainties of protein calculation and structure may rise.[69] Hence, ^{13}C-edited 3D NOESY is considered to be a complementary method that can provide additional NOE constraints.

Since NMR-based structural biology depends on NOESY to obtain structure elucidation and modeling, many new techniques have been developed over the years to maximize sensitivity and data quality and, most importantly, reduce collection time. These include newly developed 3D NOESY experiments based on fast pulsing SOFAST-HMQC, 3D SOFAST-HMQC-NOESY-HMQC, and 3D SOFAST NOESY-HMQC experiments.[99]

1.4 Summary and Future Perspectives

Here we have focused on the theory and applications of basic methods of NMR spectroscopy that have been used for sequence-specific resonance assignment followed by structure elucidation. We provided some fundamental aspects of dynamics investigation using NMR for biological molecules. One can perform NMR measurements under physiological conditions, and real-time dynamics information can be derived, which is unique to NMR. We initially discussed how historically two-dimensional (2D) NMR spectroscopy was introduced, which boosted the development of multidimensional experimental possibilities combining chemical shifts of coupled homonuclear and/or heteronuclear spins. Later, the dipolar interactions between pairs of nuclear spins were utilized to derive structural information. The details of magnetization transfer, basic building blocks for polarization transfer from one spin to other spins, were discussed at great length. We first provided a comprehensive discussion of INEPT and reverse-INEPT building blocks, which form the basis of all triple resonance experiments. The nomenclature and detailed magnetization pathways for triple resonance experiments were subsequently discussed. Numerous advances have been made during the past two decades to achieve three- and four-dimensional spectroscopy in a reasonable amount of time, and the corresponding research area for FAST NMR methodologies was introduced. We have also covered the detailed theory of dipole–dipole interaction between two spins at an advanced level. In this direction, the Nuclear Overhauser Effect (NOE) phenomenon was introduced first. This is the basic concept for probing the through-space correlations by atoms and led subsequently to different techniques to measure the distance between instigated spins, such as paramagnetic relaxation enhancement (PRE), Rotational Frame Overhauser Effect Spectroscopy (ROESY), Nuclear Overhauser Effect Spectroscopy (NOESY), and Heteronuclear Overhauser Effect Spectroscopy (HOESY or hetNOE), which were also discussed.

Thus our approach has been to provide a solid foundation for the two most important aspects of NMR. The first was the foundation of building blocks, magnetization transfer, followed by details of the structure elucidation process. Recently, selective 'labeling' and 'unlabeling' have been reported as a cost-effective method for unambiguous assignment. This has been backed by simultaneous advancement in the hardware technologies, such as the availability of higher magnetic fields, cryogenic probes, pulsed-field gradients, availability of separately controllable radiofrequency channels, *etc.* New-generation pulse programs were designed to overcome spectral degeneracy and chemical shift overlap problems for different kinds of systems. To overcome the resolution barrier, and utilize the full potential of higher magnetic fields, nonuniform sampling and associated processing algorithms have been developed. The most obvious advantage of NMR spectroscopy is that it is still the only available technique to investigate molecular dynamics at different levels, such as proteins and DNA under physiological conditions.

With advancements in the last 10 years, some new avenues have appeared for NMR, making it the only tool available for addressing some biological questions. The foremost of these is understanding the dynamic picture of the molecule on a real-time scale, which is the key to its function. The residual dipolar couplings (RDCs) also provide dynamic information at a much wider time scale along with directional information. One key advantage of NMR is that it can study proteins that are amenable to crystallization. Normally, any protein with a large intrinsic disorder region or full intrinsically disordered protein cannot be crystalized.

In fact, more than 34% of eukaryotic proteins fall in this category. These proteins can undergo disorder-to-order transition upon binding to their biological targets, which are key to their functions. These systems access dynamic structural preferences on various timescales, and NMR can obtain detailed information in terms of chemical shift assignment, chemical shift index, J-couplings, paramagnetic relaxation enhancement (PRE), and RDCs. Now all chemical reactions involve intermediates, and hence there are also different short-lived confirmations that serve the purpose in the case of a biological process, which is chains of complex chemical reactions at an atomic level. However, a detailed understanding of these intermediates remains elusive as these conformers are only transiently formed and marginally populated on the energy landscape. Initially, a series of relaxation dispersion experiments were introduced to probe these intermediates, which are often less than a few percent of the total population. From these measurements, the details of this exchange process's kinetic and thermodynamic parameters can be obtained. This involves the relative population, exchange rates, and the free energy difference. However, most importantly, the minor species' chemical shifts can be obtained. Later, chemical exchange saturation transfer (CEST) was proposed for the slow exchange process, which is more straightforward and yields the chemical shift information more directly for the minor species. Like relaxation dispersion, different kinds of

CEST experiments have also been proposed, and now even the diffusion parameters of the excited states have also been reported. The future of NMR relies on such detailed exploration of this kind of structural information that is directly connected to the function of biological systems. Therefore, NMR will continue to play a dominant role in this field.

List of Abbreviations

NMR	Nuclear Magnetic Resonance
1D	one-dimensional
2D	two-dimensional
3D and 4D	three- and four-dimensional
ROESY	Rotational Frame Overhauser Effect SpectroscopY
NOESY	Nuclear Overhauser Effect SpectroscopY
HOESY or hetNOE	Heteronuclear Overhauser Effect SpectroscopY

References

1. M. Bauer, A. Bertario, G. Boccardi, X. Fontaine, R. Rao and D. Verrier, *J. Pharm. Biomed. Anal.*, 1998, **17**, 419–425.
2. M.-E. Dumas, E. C. Maibaum, C. Teague, H. Ueshima, B. Zhou, J. C. Lindon, J. K. Nicholson, J. Stamler, P. Elliott and Q. Chan, *Anal. Chem.*, 2006, **78**, 2199–2208.
3. A.-H. Emwas, R. Roy, R. T. McKay, L. Tenori, E. Saccenti, G. Gowda, D. Raftery, F. Alahmari, L. Jaremko and M. Jaremko, *Metabolites*, 2019, **9**, 123.
4. C. A. Blindauer, A. H. Emwas, A. Holý, H. Dvořáková, E. Sletten and H. Sigel, *Chem. Eur. J.*, 1997, **3**, 1526–1536.
5. B. Davaasuren, A.-H. Emwas and A. Rothenberger, *Inorg. Chem.*, 2017, **56**, 9609–9616.
6. M. Huang, S. Chen, J. Huang, R. E. Gerald II and K. Woelk, *Mater. Sci. Eng. C*, 2020, 111177.
7. E. Steimers, Y. Matviychuk, A. Friebel, K. Münnemann, E. von Harbou and D. J. Holland, *Magn. Reson. Chem.*, 2020, **59**, 221–236.
8. J. Aburabie, A. H. Emwas and K. V. Peinemann, *Macromol. Mater. Eng.*, 2019, **304**, 1800551.
9. S. Asghar, T. Shahzadi, M. Alazmi, X. Gao, A.-H. Emwas, R. S. Saleem, F. Batool and G. A. Chotana, *Synthesis*, 2018, **50**, 2211–2220.
10. A. G. A. Jameel, N. Naser, A.-H. Emwas and S. M. Sarathy, *Proc. Combust. Inst.*, 2019, **37**, 4663–4671.
11. A. G. A. Jameel, N. Naser, G. Issayev, J. Touitou, M. K. Ghosh, A.-H. Emwas, A. Farooq, S. Dooley and S. M. Sarathy, *Combust. Flame*, 2018, **192**, 250–271.
12. S. Manzoor, A. Bilal, S. Khan, R. Ullah, S. Iftikhar, A.-H. Emwas, M. Alazmi, X. Gao, A. Jawaid and R. S. Z. Saleem, *Sci. Rep.*, 2018, **8**, 1–12.

13. A. O'Rourke, S. Kremb, B. M. Duggan, S. Sioud, N. Kharbatia, M. Raji, A.-H. Emwas, W. H. Gerwick and C. R. Voolstra, *Molecules*, 2018, **23**, 1472.
14. Z. U. Rehman, S. Jeong, S. Tabatabai, A. Emwas and T. Leiknes, *Desalin. Water Treat.*, 2017, **69**, 1–11.
15. G. Zhang, A.-H. Emwas, U. F. S. Hameed, S. T. Arold, P. Yang, A. Chen, J.-F. Xiang and N. M. Khashab, *Chem.*, 2020, **6**, 1082–1096.
16. D. Hüse, L. Bíró, J. Patalenszki, A. C. Bényei and P. Buglyó, *Eur. J. Inorg. Chem.*, 2014, **2014**, 5204–5216.
17. N. H. Ahmed, G. R. Saad and M. M. Naoum, *Liq. Cryst.*, 2018, **45**, 1487–1497.
18. P. Agback, E. Woestenenk and T. Agback, *BMC Mol. Cell Biol.*, 2020, **21**, 1–15.
19. J. Deng, T. Ma, Z. Chang, W. Zhao and J. Yang, *Acta Phys.-Chim. Sin.*, 2020, **36**, 1901079.
20. J. M. Oommen, M. M. Hussain, A.-H. M. Emwas, P. Agarwal and L. A. Archer, *Electrochem. Solid-State Lett.*, 2010, **13**, K87.
21. S. Chu, S. Maltsev, A.-H. Emwas and G. A. Lorigan, *J. Magn. Reson.*, 2010, **207**, 89–94.
22. S. Li, O. Lafon, W. Wang, Q. Wang, X. Wang, Y. Li, J. Xu and F. Deng, *Adv. Mater.*, 2020, 2002879.
23. P. Rovó, *Solid State Nucl. Magn. Reson.*, 2020, 101665.
24. G. Qi, Y. Chu, Q. Wang, X. Wang, Y. Li, J. Trébosc, O. Lafon, J. Xu and F. Deng, *Angew. Chem., Int. Ed.*, 2020, **132**, 19700–19706.
25. F. Alahmari, B. Davaasuren, A.-H. Emwas and A. Rothenberger, *Inorg. Chem.*, 2018, **57**, 3713–3719.
26. S. Asghar, T. Shahzadi, M. Alazmi, X. Gao, A. H. Emwas, R. S. Z. Saleem, F. Batool and G. A. Chotana, *Synthesis*, 2018, **50**, 2211–2220.
27. T. F. Huang, G. Sheng, P. Manchanda, A. H. Emwas, Z. P. Lai, S. P. Nunes and K. V. Peinemann, *Sci. Adv.*, 2019, **5**, eaax6976.
28. A. G. A. Jameel, A. Khateeb, A. M. Elbaz, A. H. Emwas, W. Zhang, W. L. Roberts and S. M. Sarathy, *Fuel*, 2019, **253**, 950–963.
29. X. H. Qiu, D. Redwine, K. Beshah, S. Livazovic, C. G. Canlas, A. Guinov and A. H. M. Emwas, *J. Membr. Sci.*, 2019, **581**, 243–251.
30. N. Glanzmann, A. M. L. Carmo, L. M. R. Antinarelli, E. S. Coimbra, L. A. S. Costa and A. D. da Silva, *J. Mol. Model.*, 2018, **24**, 160.
31. R. A. Hill and C. P. Nicholson, *J. Chem. Educ.*, 2017, **94**, 1965–1968.
32. R. Hopson, P. Y. B. Lee and K. M. Hess, *J. Chem. Educ.*, 2018, **95**, 641–647.
33. F. Alahmari, B. Davaasuren, A. H. Emwas, P. Costa and A. Rothenberger, *Inorg. Chim. Acta*, 2019, **488**, 145–151.
34. M. Alghrably, D. Dudek, A. H. Emwas, L. Jaremko, M. Jaremko and M. Rowinska-Zyrek, *Inorg. Chem.*, 2020, **59**, 2527–2535.
35. R. A. Alsiary, M. Alghrably, A. Saoudi, S. Al-Ghamdi, L. Jaremko, M. Jaremko and A. H. Emwas, *Neurol. Sci.*, 2020, **41**, 2389–2406.
36. Z. A. Al-Talla, S. H. Akrawi and A. H. M. Emwas, *Int. J. Clin. Pharmacol. Ther.*, 2011, **49**, 469–476.

37. C. M. Davis and B. M. Dixon, *J. Chem. Educ.*, 2011, **88**, 309–310.
38. L. Ronconi and P. J. Sadler, *Coord. Chem. Rev.*, 2008, **252**, 2239–2277.
39. K. Srikanth, R. W. Schurko, I. Hung and A. Ramamoorthy, *Mater. Sci. Technol.*, 2003, **19**, 1191–1196.
40. S. Appelt, A. Kentner, S. Lehmkuhl and B. Blumich, *Prog. Nucl. Magn. Reson. Spectrosc.*, 2019, **114**, 1–32.
41. D. R. Glenn, D. B. Bucher, J. Lee, M. D. Lukin, H. Park and R. L. Walsworth, *Nature,*, 2018, **555**, 351–354.
42. M. Jiang, J. Bian, X. M. Liu, H. Y. Wang, Y. L. Ji, B. Zhang, X. H. Peng and J. F. Du, *Phys. Rev. A*, 2018, **97**, 062118.
43. L. Shen and L. M. Peng, *Chin. J. Catal.*, 2015, **36**, 1494–1504.
44. S. Ciambellotti and P. Turano, *Eur. J. Inorg. Chem.*, 2019, 569–576.
45. A. Marchanka and T. Carlomagno, in *Biological Nmr, Pt B*, 2019, ed. A. J. Wand, vol. 615, pp. 333–371.
46. N. Nishida, Y. Ito and I. Shimada, *Biochim. Biophys. Acta, Gen. Subj.*, 2020, **1864**, 129364.
47. J. Bernarding, F. Euchner, C. Bruns, R. Ringleb, D. Muller, T. Trantzschel, J. Bargon, U. Bommerich and M. Plaumann, *Chem. Phys. Chem.*, 2018, **19**, 2453–2456.
48. J. H. Du and L. M. Peng, *Chin. Chem. Lett.*, 2018, **29**, 747–751.
49. A. M. Olaru, T. B. R. Robertson, J. S. Lewis, A. Antony, W. Iali, R. E. Mewis and S. B. Duckett, *ChemistryOpen*, 2018, **7**, 97–105.
50. M. Pellecchia, I. Bertini, D. Cowburn, C. Dalvit, E. Giralt, W. Jahnke, T. L. James, S. W. Homans, H. Kessler and C. Luchinat, *Nat. Rev. Drug Discovery*, 2008, **7**, 738–745.
51. E. A. Mahrous and M. A. Farag, *J. Adv. Res.*, 2015, **6**, 3–15.
52. G. M. Clore and A. M. Gronenborn, *Annu. Rev. Biophys. Biophys. Chem.*, 1991, **20**, 29–63.
53. L. E. Kay, G. M. Clore, A. BAx and A. M. Gronenborn, *Science*, 1990, **249**, 411–414.
54. A.-H. Emwas, K. Szczepski, B. G. Poulson, K. Chandra, R. T. McKay, M. Dhahri, F. Alahmari, L. Jaremko, J. I. Lachowicz and M. Jaremko, *Molecules*, 2020, **25**, 4597.
55. J. Jeener and G. Alewaeters, *Prog. Nucl. Magn. Reson. Spectrosc.*, 2016, **94**, 75–80.
56. K. Anil, R. R. Ernst and K. Wüthrich, *Biochem. Biophys. Res. Commun.*, 1980, **95**, 1–6.
57. M. P. Williamson, T. F. Havel and K. Wüthrich, in *Nmr In Structural Biology: A Collection of Papers by Kurt Wüthrich*, World Scientific, 1995, pp. 319–339.
58. J. Ying, F. Delaglio, D. A. Torchia and A. Bax, *J. Biomol. NMR*, 2017, **68**, 101–118.
59. M. A. Thomas, R. Nagarajan, A. Huda, D. Margolis, M. K. Sarma, K. Sheng, R. E. Reiter and S. S. Raman, *NMR Biomed.*, 2014, **27**, 53–66.
60. E. Kupče and R. Freeman, *J. Biomol. NMR*, 2004, **28**, 391–395.
61. M. Zinke, P. Fricke, C. Samson, S. Hwang, J. S. Wall, S. Lange, S. Zinn-Justin and A. Lange, *Angew. Chem., Int. Ed.*, 2017, **56**, 9497–9501.

62. A.-H. Emwas, M. Alghrably, S. Al-Harthi, B. G. Poulson, K. Szczepski, K. Chandra and M. Jaremko, in *Nuclear Magnetic Resonance*, ed. N. Khaneja, IntechOpen, London, UK, 2019, ch. 5, pp. 83–106.
63. Ē. Kupče, K. R. Mote and P. K. Madhu, *J. Magn. Reson.*, 2019, **304**, 16–34.
64. R. A. Alsiary, M. Alghrably, A. Saoudi, S. Al-Ghamdi, L. Jaremko, M. Jaremko and A.-H. Emwas, *Neurol. Sci.*, 2020, 1–18.
65. G. Wagner, A. Kumar and K. Wüthrich, *Eur. J. Biochem.*, 1981, **114**, 375–384.
66. W. C. Johnson Jr, T. G. Pagano, C. T. Basson, J. A. Madri, P. Gooley and I. M. Armitage, *Biochemistry*, 1993, **32**, 268–273.
67. G. M. Clore, A. Bax, P. C. Driscoll, P. T. Wingfield and A. M. Gronenborn, *Biochemistry*, 1990, **29**, 8172–8184.
68. P. C. Driscoll, G. M. Clore, D. Marion, P. T. Wingfield and A. M. Gronenborn, *Biochemistry*, 1990, **29**, 3542–3556.
69. J. Cavanagh, W. J. Fairbrother, A. G. Palmer III and N. J. Skelton, *Protein NMR Spectroscopy: Principles and Practice*, Elsevier, 2nd edn., 2007.
70. J. Cavanagh, W. J. Fairbrother, A. G. Palmer III and N. J. Skelton, *Protein NMR Spectroscopy: Principles and Practice*, Elsevier, 1995.
71. M. P. Williamson and J. P. Waltho, *Chem. Soc. Rev.*, 1992, **21**, 227–236.
72. L. E. Kay, L. K. Nicholson, F. Delaglio, A. Bax and D. Torchia, *J. Magn. Reson. (1969)*, 1992, **97**, 359–375.
73. O. Zhang, L. E. Kay, J. P. Olivier and J. D. Forman-Kay, *J. Biomol. NMR*, 1994, **4**, 845–858.
74. N. A. Farrow, R. Muhandiram, A. U. Singer, S. M. Pascal, C. M. Kay, G. Gish, S. E. Shoelson, T. Pawson, J. D. Forman-Kay and L. E. Kay, *Biochemistry*, 1994, **33**, 5984–6003.
75. D. Muhandiram, G. Y. Xu and L. E. Kay, *J. Biomol. NMR*, 1993, **3**, 463–470.
76. M. Nowakowski, Ł. Jaremko, M. Jaremko, I. Zhukov, A. Belczyk, A. Bierzyński and A. Ejchart, *J. Struct. Biol.*, 2011, **174**, 391–399.
77. M. Jaremko, Ł. Jaremko, H.-Y. Kim, M.-K. Cho, C. D. Schwieters, K. Giller, S. Becker and M. Zweckstetter, *Nat. Chem. Biol.*, 2013, **9**, 264–270.
78. A. W. Overhauser, *Phys. Rev.*, 1953, **92**, 411–415.
79. J. Fattori, F. H. S. Rodrigues, J. G. M. Pontes, A. Paula Espíndola and L. Tasic, in *Applications of NMR Spectroscopy: Volume 3*, ed. A. ur-Rahman and M. I. Choudhary, Bentham Science Publishers, 2015, pp. 180–266.
80. N. Wang, X. Dong, L. Liu, D. Cai, Q. Cheng, J. Wang, Y. Hou, A.-H. Emwas, J. Gascon and Y. Han, *Cell Rep. Phys. Sci.*, 2021, **2**, 100309.
81. M. P. Williamson, in *Annual Reports on NMR Spectroscopy*, Academic Press, 2009, vol. 65, pp. 77–109.
82. F. Ni, *Prog. Nucl. Magn. Reson. Spectrosc.*, 1994, **26**, 517–606.
83. A. T. Brünger, P. Adams, G. M. Clore, W. L. DeLano, P. Gros, R. W. Grosse-Kunstleve, J. Jiang, J. J. Kuszewski, M. Nilges, N. S. Pannu, R. J. Read, L. L. M. Rice, T. Simonson and G. Warren, *Acta Crystallogr., Sect. D: Biol. Crystallogr.*, 1998, **54**, 905–921.

84. G. A. Morris, *Magn. Reson. Chem.*, 1990, **28**, 738.
85. V. J. H. N. U. R. E. Schirmer, Academic Press, New York, 1971.
86. R. R. Gil and A. Navarro-Vázquez, in *Modern NMR Approaches to the Structure Elucidation of Natural Products: Volume 2: Data Acquisition and Applications to Compound Classes*, The Royal Society of Chemistry, 2017, vol. 2, pp. 1–38.
87. Eds. W. M.P., Webb G. A., *Modern Magnetic Resonance*, Springer, Dordrecht, 2008.
88. C. Karunakaran, P. Santharaman and M. Balamurugan, in *Spin Resonance Spectroscopy*, ed. C. Karunakaran, Elsevier, 2018, pp. 49–110.
89. T. D. W. Claridge, in *High-Resolution NMR Techniques in Organic Chemistry*, ed. T. D. W. Claridge, Elsevier, Boston, 3rd edn, 2016, pp. 315–380.
90. R. Atta ur, M. I. Choudhary and W. Atia tul, in *Solving Problems with NMR Spectroscopy* 2nd edn, 2016, eds. R. Atta ur, M. I. Choudhary and W. Atia tul, Academic Press, Boston, pp. 227–264.
91. E. Hatzakis, *Compr. Rev. Food Sci. Food Saf.*, 2019, **18**, 189–220.
92. M. J. Howard, *Curr. Biol.*, 1998, **8**, R331–R333.
93. S. H. Mishra, B. J. Harden and D. P. Frueh, *J. Biomol. NMR*, 2014, **60**, 265–274.
94. C. Yu and G. C. Levy, *J. Am. Chem. Soc.*, 1984, **106**, 6533–6537.
95. J. H. Simpson, in *Organic Structure Determination Using 2-D NMR Spectroscopy*, ed. J. H. Simpson, Academic Press, Boston, 2nd edn, 2012, pp. 169–184.
96. M. J. Sweredoski, K. J. Donovan, B. D. Nguyen, A. J. Shaka and P. Baldi, *Bioinformatics*, 2007, **23**, 2829–2835.
97. H. Oschkinat, C. Griesinger, P. J. Kraulis, O. W. Sørensen, R. R. Ernst, A. M. Gronenborn and G. M. Clore, *Nature*, 1988, **332**, 374–376.
98. P. Schmieder, in *Encyclopedic Reference of Genomics and Proteomics in Molecular Medicine*, Springer Berlin Heidelberg, Berlin, Heidelberg, 2006, pp. 1204–1208.
99. P. Rossi, Y. Xia, N. Khanra, G. Veglia and C. Kalodimos, *J. Biomol. NMR*, 2016, **66**, 259–271.